ENGINEERING

Ultrahigh-efficiency solution-processed simplified small-molecule organic light-emitting diodes using universal host materials

Tae-Hee Han,[1,2] Mi-Ri Choi,[1] Chan-Woo Jeon,[3] Yun-Hi Kim,[3]* Soon-Ki Kwon,[4] Tae-Woo Lee[2]*

Although solution processing of small-molecule organic light-emitting diodes (OLEDs) has been considered as a promising alternative to standard vacuum deposition requiring high material and processing cost, the devices have suffered from low luminous efficiency and difficulty of multilayer solution processing. Therefore, high efficiency should be achieved in simple-structured small-molecule OLEDs fabricated using a solution process. We report very efficient solution-processed simple-structured small-molecule OLEDs that use novel universal electron-transporting host materials based on tetraphenylsilane with pyridine moieties. These materials have wide band gaps, high triplet energy levels, and good solution processabilities; they provide balanced charge transport in a mixed-host emitting layer. Orange-red (~97.5 cd/A, ~35.5% photons per electron), green (~101.5 cd/A, ~29.0% photons per electron), and white (~74.2 cd/A, ~28.5% photons per electron) phosphorescent OLEDs exhibited the highest recorded electroluminescent efficiencies of solution-processed OLEDs reported to date. We also demonstrate a solution-processed flexible solid-state lighting device as a potential application of our devices.

INTRODUCTION

Organic light-emitting diodes (OLEDs) have various applications, such as next-generation flat-panel displays and solid-state lighting sources (*1*–*6*). The standard method to fabricate OLEDs is vacuum thermal deposition, but this method is expensive and uses materials inefficiently. Therefore, a solution process to fabricate organic/polymeric emitting and transporting materials is in great demand for low-cost, large-area production of OLEDs by using inkjet printing or roll-to-roll printing (*7*–*11*).

Polymeric emitting layers (EMLs) have good solution processability and multifunctionality and thus have often been used in solution-processed OLEDs (*12*–*14*). However, achieving polymer LEDs with luminous efficiencies that are comparable to those of state-of-the-art vacuum-deposited small-molecule OLEDs remains a major challenge. As an alternative material for fabrication of solution-processed OLEDs, small-molecule conjugated materials can be a good option because of their advantages of facile synthesis and purification, and monodispersed molecular weight (*8*, *9*). Recently, solution-processed OLEDs have been fabricated using small-molecule host materials doped with fluorescent or phosphorescent emitters (*15*–*26*), but these devices have lower luminous efficiencies than state-of-the-art vacuum-deposited OLEDs.

Vacuum-deposited small-molecule OLEDs with multilayered structures have been developed; these structures include charge-transporting layers to achieve balanced charge transport and exciton confinement. However, the solution process of small molecules dissolved in organic solvents to fabricate multilayers of small molecules encounters major difficulties because of redissolution of underlying layers. This problem can be avoided by developing a method to realize highly efficient solution-processed small-molecule OLEDs with a simple device structure. Therefore, the EML of simple-structured OLEDs should meet several requirements, including balanced charge-carrier transport and exciton confinement for radiative exciton recombination. In addition, the host materials should provide efficient energy transfer to red, green, and blue phosphorescent dopant materials to realize large-area, full-color displays and solid-state lighting devices at a low cost.

To fulfill these requirements, we designed new tetrahedral silicon-based hosts, which are composed of a central Si atom with a 3d orbital, and a phenyl or *m*-pyridyl phenyl moiety. The tetrahedral configurations with two meta-pyridine substituents give it good morphological stability and solubility (*27*, *28*). In addition, 3d-π interaction between the central Si atom and the phenyl or pyridyl phenyl group without disconnection of conjugation at the Si atom yields a wide band gap and high T1 state for a blue phosphorescent host. Pyridyl-substituted hosts have a high electron-transporting ability and can therefore achieve balanced charge-carrier transport.

RESULTS

We synthesized electron-transporting host materials for solution-processed phosphorescent orange-red, green, blue, and white OLEDs; these materials are diphenylbis(3-(pyridine-2-yl)phenyl)silane (2PTPS), diphenylbis(3-(pyridine-3-yl)phenyl)silane (3PTPS), and diphenylbis(3-(pyridine-4-yl)phenyl)silane (4PTPS) with the pyridine moieties in various orientations (Fig. 1). Synthesis of 2PTPS, 3PTPS, and 4PTPS began with lithiation of 1,3-dibromobenzene by using *n*-butyllithium and subsequent treatment with dichlorodiphenylsilane to give bis(3-bromophenyl)diphenylsilane. 2PTPS was synthesized by Stille cross-coupling reaction between 2-(tributylstannyl)pyridine and bis(3-bromophenyl)diphenylsilane. 3PTPS and 4PTPS were synthesized by Suzuki cross-coupling reaction between pyridineboronic acid and bis(3-bromophenyl)diphenylsilane. The identities of 2PTPS, 3PTPS, and 4PTPS were confirmed using nuclear magnetic resonance (NMR) and mass analysis (Supplementary Materials). 2PTPS, 3PTPS,

[1]Department of Materials Science and Engineering, Pohang University of Science and Technology, 77 Cheongam-Ro, Nam-Gu, Pohang, Gyungbuk 790-784, Republic of Korea. [2]Department of Materials Science and Engineering, Seoul National University, 1 Gwanak-ro, Gwanak-gu, Seoul 08826, Republic of Korea. [3]Department of Chemistry and Research Institute of Natural Science, Gyeongsang National University, Gyeongnam, Republic of Korea. [4]School of Materials Science and Engineering and Engineering Research Institute, Gyeongsang National University, Gyeongnam, Republic of Korea.
*Corresponding author. Email: twlees@snu.ac.kr (T.-W.L.); ykim@gnu.ac.kr (Y.-H.K.)

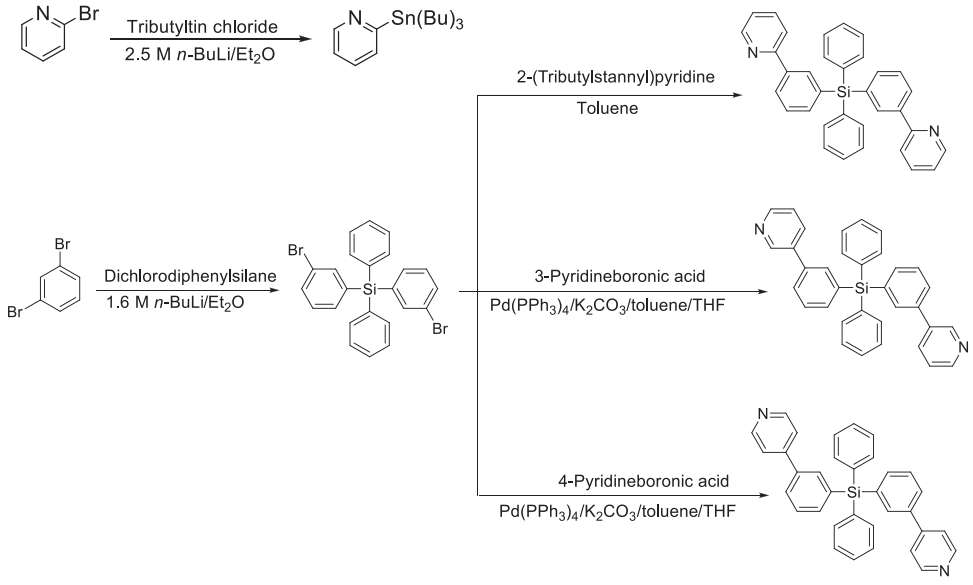

Fig. 1. Synthesis routes of 2PTPS, 3PTPS, and 4PTPS.

and 4PTPS have high thermal stability with high glass transition temperature (T_g) (table S1).

To measure the electrochemical properties and energy levels of materials, we performed cyclic voltammetry (CV) in a conventional three-electrode configuration in acetonitrile containing 0.1 M tetrabutylammonium perchlorate (Bu_4NClO_4) as the supporting electrolyte versus an Ag/AgCl platinum disc as the working electrode and platinum wire as the counter electrode (fig. S1). The estimated highest occupied molecular orbital (HOMO) levels of 2PTPS, 3PTPS, and 4PTPS were −6.47, −6.50, and −6.55 eV, respectively, and the lowest unoccupied molecular orbital (LUMO) levels were −2.41, −2.30, and −2.27 eV, respectively (Table 1 and figs. S1 to S4). Lower HOMO and higher LUMO energies of the host than the corresponding energies of the blue phosphorescent dopant molecule {bis[2-(4,6-difluorophenyl)pyridinato-N, C2] (picolinato)iridium (FIrpic), −5.90 and −3.00 eV} are expected to favor energy transfer from the host to the emitting dopant. Phosphorescence of 2PTPS, 3PTPS, and 4PTPS was measured in a $CHCl_3$ matrix at 77 K (fig. S5). The highest-energy 0-0 phosphorescent emissions located at 2.82, 2.82, and 2.90 eV for 2PTPS, 3PTPS, and 4PTPS, respectively, were used to calculate their triplet energy (E_T) gaps (Table 1). E_T's of the new host materials are higher than those of the conventional blue dopant, FIrpic (~2.7 eV) (*29*), and sufficient for them to serve as suitable host materials for blue phosphorescent dopant. For a favorable radiative exciton recombination without backward energy transfer from dopant to host, host materials should have higher E_T than the blue-emitting phosphorescent dopant (*29*).

To achieve highly efficient simple-structured OLEDs without additional hole-transporting or electron-blocking interfacial layers, we used two approaches in this work: (i) a high work function solution-processed hole injection layer (HIL) that blocks exciton quenching at the HIL/EML interface (*30*) and (ii) a mixed-host EML that consists of electron- and hole-transporting host materials. Because host materials in the EML have deep HOMO energy levels [for example, 4,4′,4′′-tris(*N*-carbazolyl)-triphenylamine (TCTA) ~−5.7 to 5.9 eV], the large energy barrier at the HIL/EML interface must be overcome to achieve balanced charge injection to the EML without the need for an additional hole-transporting interlayer. Therefore, we used a polymeric HIL, which develops a gradient work function that increases from the anode to the top surface of the HIL by self-organization and that has a very high surface work function (~5.95 eV) (figs. S6 and S7 and table S2). Our gradient HIL (GraHIL) is composed of conventional conducting polymer, poly(3,4-ethylenedioxythiophene) doped with poly(styrenesulfonate) (PEDOT/PSS), and tetrafluoroethylene-perfluoro-3,6-dioxa-4-methyl-7-octenesulfonic acid copolymer [a perfluorinated ionomer (PFI)] in 1:3.6 weight ratio. The GraHIL facilitates hole injection from the anode to an overlying EML by reducing the large energy barrier between the anode and the EML in the simple structure. In addition, enrichment of PFI in the surface layer effectively blocks exciton quenching at the HIL/EML interface (*30*, *31*). The solution-processed EML consists of a 1:1 weight mixture of a hole-transporting host material (TCTA) and an electron-transporting host material, which is selected from among 2PTPS, 3PTPS, 4PTPS, or conventionally used solution-processable small-molecule host material {2,2,2-(1,3,5-benzenetriyl)tris-[1-phenyl-1*H*-benzimidazole] (TPBI)}. The bipolar mixed-host EML consists of electron- and hole-transporting hosts to facilitate charge-carrier injection to the EML and balanced charge transport to a recombination zone in the EML (*32*, *33*). In addition, the bipolar characteristics of this mixed-host system easily distribute excitons in

Table 1. Physical properties of electron-transporting host materials.

	HOMO (eV)	Δ*E* (eV)	LUMO (eV)	E_T (eV)
2PTPS	−6.47	4.06	−2.41	2.82
3PTPS	−6.50	4.20	−2.30	2.82
4PTPS	−6.55	4.28	−2.27	2.90
TPBI	−6.40	3.30	−2.70	2.70

the EML over a broad recombination zone that can effectively avoid nonradiative exciton quenching, such as triplet-triplet annihilation and triplet-polaron annihilation (*32*, *33*).

To evaluate our phosphorescent host materials, we fabricated simple-structured orange-red, green, and blue phosphorescent OLEDs (Fig. 2A) based on phosphorescent dopants, bis(2-phenyl benzothiozolato-*N*,$C^{2'}$)iridium(acetylacetonate) [$Bt_2Ir(acac)$], tris[2-phenylpyridinato-C^2,*N*]iridium(III) [$Ir(ppy)_3$], and FIrpic, respectively. Compared to devices with a conventional electron-transporting host (TPBI), all $Bt_2Ir(acac)$-based orange-red phosphorescent OLEDs with our novel tetraphenylsilane host exhibited superior electrical and luminescent characteristics (Fig. 2, B and C). Solution-processed orange-red phosphorescent OLEDs with our host materials achieved much higher luminous current efficiencies (CEs) and external quantum efficiencies (EQEs) (device with 2PTPS ~95.7 cd/A, 35.4%; 3PTPS ~97.5 cd/A, 35.5%; 4PTPS ~76.4 cd/A, 28.0%) than did those with TPBI (~60.6 cd/A, 21.2%) (Fig. 2C, figs. S8 to S10, and Table 2). These high electroluminescent efficiencies of orange-red OLEDs can originate from the chemical structure of phosphorescent emitter molecule [$Bt_2Ir(acac)$], in which the orientation of the transition dipole moment is preferentially horizontal (*34*). OLEDs that use an EML in which emitter molecules are aligned horizontally have higher optical outcoupling efficiency than those that use an EML in which emitter molecules are distributed isotropically (*34*–*36*). A possible additional source of increased electroluminescent efficiency is a weak microcavity effect caused by the combination of the low refractive index of the GraHIL (n ~1.4) and the high refractive index of indium tin oxide (ITO) (n ~1.9) in our device architecture (*37*). Devices with 2PTPS and

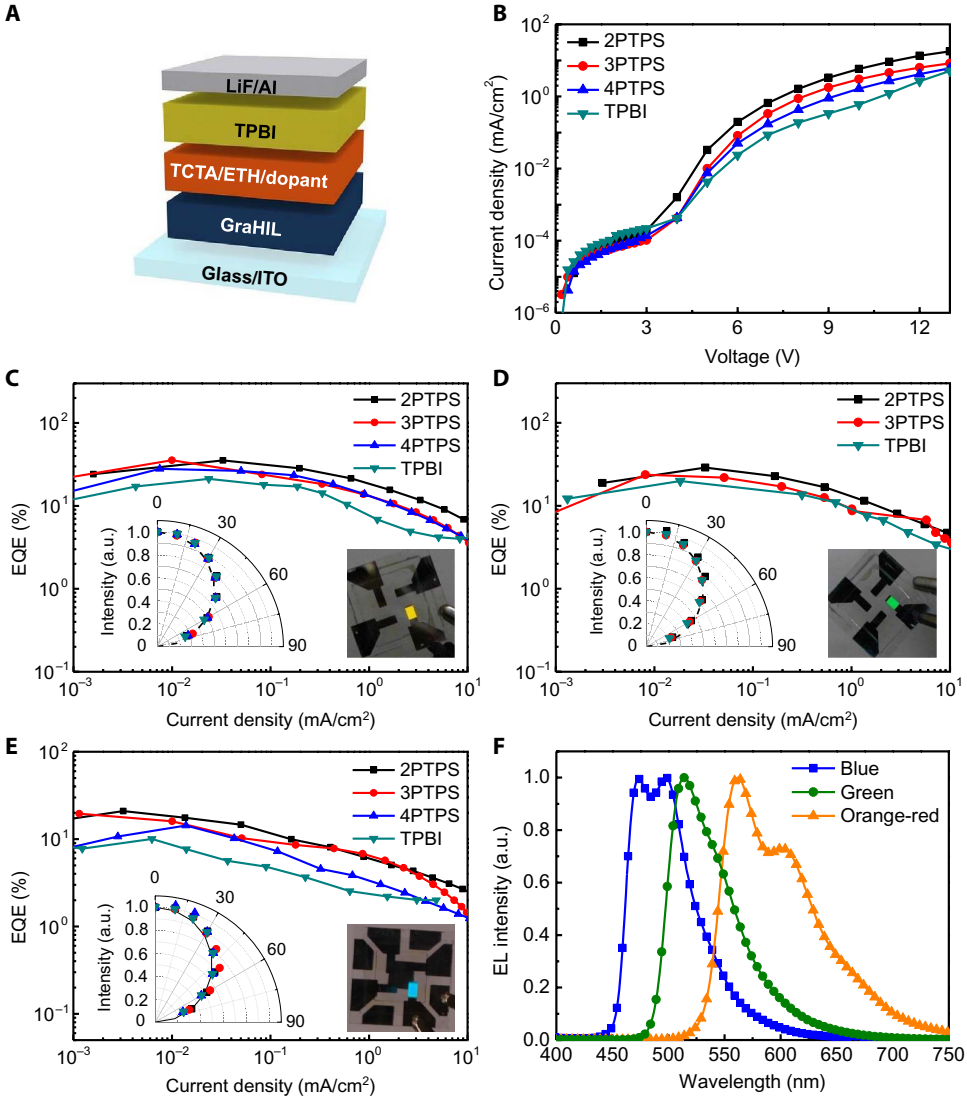

Fig. 2. Electrical and electroluminescent characteristics of solution-processed orange-red, green, and blue phosphorescent OLEDs. (**A**) Architecture of solution-processed phosphorescent OLED devices. (**B**) Current density versus voltage characteristics of phosphorescent orange-red OLEDs with various electron-transporting host materials. EQEs versus current density characteristics of $Bt_2Ir(acac)$-based orange-red (**C**), $Ir(ppy)_3$-based green (**D**), and FIrpic-based blue (**E**) OLEDs with various electron-transporting host materials. (C to E) (Insets) Left: angular electroluminescence (EL) distributions according to viewing angle; right: photographs of devices and their color emission. (**F**) EL spectra of solution-processed OLEDs with 2PTPS. a.u., arbitrary units.

Table 2. Device efficiencies of solution-processed OLEDs.

	CE_{max} (cd/A)	EQE_{max} (%)
2PTPS		
Orange	95.7	35.4
Green	101.5	29.0
Blue	38.7	20.9
White	61.5	23.1
3PTPS		
Orange	97.5	35.5
Green	88.5	23.7
Blue	32.6	19.6
White	74.2	28.5
4PTPS		
Orange	76.4	28.0
Green	—	—
Blue	28.8	14.3
White	—	—
TPBI		
Orange	60.6	21.2
Green	79.5	19.9
Blue	18.6	10.0
White	40.5	15.4

3PTPS showed better electrical characteristics and higher efficiencies than did those with 4PTPS. Therefore, we also fabricated $Ir(ppy)_3$-based green phosphorescent OLEDs with 2PTPS and 3PTPS. Green-emitting devices that used our host materials also exhibited very high device efficiencies (device with 2PTPS ~101.5 cd/A, 29.0%; 3PTPS ~88.5 cd/A, 23.7%), which were also higher than those with TPBI (~79.5 cd/A, 19.9%) (Fig. 2D, fig. S10, and Table 2). These very high CEs and EQEs of orange-red and green phosphorescent OLEDs are the highest recorded in solution-processed orange-red and green OLEDs to date, thereby demonstrating the great potential of solution-processed small-molecule OLEDs in a simplified structure for low-cost applications. Because the introduced pyridine moieties are connected to the tetraphenylsilane moieties at their meta-position to minimize the conjugation length, our electron-transporting host materials have a wide energy gap and high E_T (>2.8 eV), which are suitable for blue-emitting phosphorescent OLEDs. The FIrpic-based solution-processed phosphorescent blue OLEDs showed higher contrast between efficiencies of devices with our host materials (device with 2PTPS ~38.7 cd/A, 20.9%; 3PTPS ~32.6 cd/A, 19.6%; 4PTPS ~28.8 cd/A, 14.3%) and those with TPBI (~18.6 cd/A, 10.0%) than did those of other color-emitting devices (Fig. 2E, fig. S10, and Table 2). The larger difference between blue OLEDs with our host materials and those with TPBI than the differences between green and orange-red OLEDs with our host materials and those with TPBI can be attributed to an additional origin: the higher E_T of our host materials, which can serve effective triplet exciton confinement on a phosphorescent dopant by blocking backward energy transfer to host materials (FIrpic, E_T ~2.7 eV) (*32*, *33*). The peaks in the EL spectra of OLEDs with 2PTPS were at ~563 nm in the $Bt_2Ir(acac)$-based orange-red OLED, at ~513 nm in the $Ir(ppy)_3$-based green OLED, and at ~472 nm in the FIrpic-based blue-emitting OLED (Fig. 2F).

The conventional TCTA/TPBI mixed-host forms exciplexes by intermolecular interaction, and its major recombination mechanism is energy transfer from the exciplexes to phosphorescent dopants (figs. S11 to S13) (*38*–*40*). In contrast, the dominant exciton generation mechanism of exciplex-free TCTA/2PTPS is direct recombination in phosphorescent dopants by charge-carrier trapping on dopant molecules (figs. S11 to S13). Direct charge injection and trapping on phosphorescent dopants in TCTA/2PTPS facilitate balanced charge transport and efficient direct recombination in TCTA/2PTPS mixed-host EML (fig. S13) (*39*–*42*). Relatively low electroluminescent efficiencies of blue phosphorescent OLEDs that use FIrpic occur because it has a deeper HOMO energy level (−5.9 eV) than $Bt_2Ir(acac)$ (−5.6 eV) and $Ir(ppy)_3$ (−5.2 eV) (*43*–*45*). The deepest HOMO energy level of FIrpic reduces hole injection from HIL, whereas $Ir(ppy)_3$ and $Bt_2Ir(acac)$ have shallower HOMO energy levels than the host materials and therefore facilitate hole injection by direct injection of holes to the dopants (figs. S14 to S16). The reduction in hole injection can cause a charge imbalance in EML and thereby reduce device efficiencies of OLEDs.

To investigate electrical properties of devices with various electron-transporting hosts, we performed several kinds of electrical analyses. The capacitance-voltage (*C*-*V*) characterization of OLEDs provides information about injection and accumulation of charge carriers under varying applied voltages. A sharp increase of capacitance at low voltage suggests accumulation of major charge carriers that have been injected and transported from the electrode to the EML (*45*). The accumulated major charge carriers start recombining with injected minor carriers at high voltage, so the capacitance between electrodes starts decreasing (*46*, *47*). Solution-processed phosphorescent orange-red OLED with 2PTPS exhibited peak capacitance at the lowest voltage (Fig. 3A); this result implies that OLEDs with 2PTPS/TCTA EML have the fastest charge transport and best-balanced electron-hole recombination, so they had both the lowest operating voltages and the highest device efficiencies of OLEDs (Fig. 2, B and C). The voltage of the peak capacitance (V_{peak}) of the devices with 2PTPS, 3PTPS, 4PTPS, and TPBI increased in the order 2PTPS < 3PTPS < 4PTPS < TPBI (Fig. 3A).

To prove that the use of electron-transporting host materials affected both the electrical and luminescent properties of solution-processed OLEDs, we also performed transient EL characterization (Fig. 3B). Transient increase of EL signal directly represents the charge transporting and recombination characteristics while an applied voltage pulse causes OLEDs to emit light. EL increased much faster with our host materials than it did with the TPBI; this means that they have better electron-transporting capability than the TPBI. Because delayed electron transport shifts the recombination zone toward the cathode, the traveling distance of the holes is extended in OLEDs; this increase in traveling distance of hole carriers delays the increase in EL during transient EL characterization. Therefore, the results of transient EL also imply that TCTA/2PTPS, TCTA/3PTPS, or TCTA/4PTPS mixed-host EMLs have better electron-transporting capability than TCTA/TPBI EML in solution-processed OLEDs.

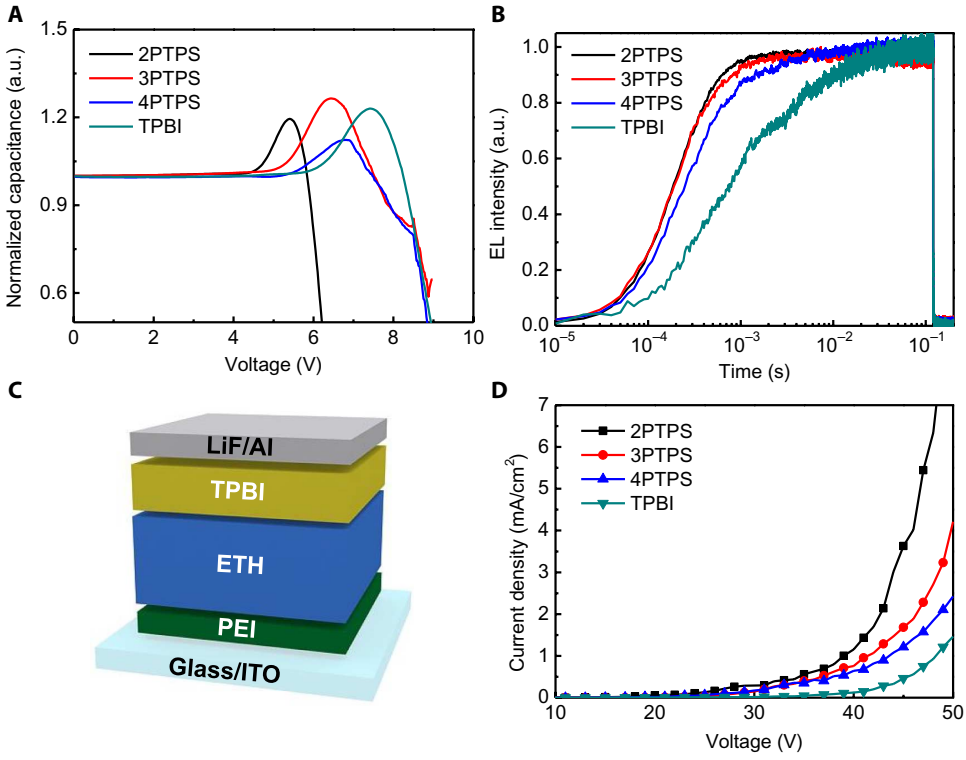

Fig. 3. Characterizations of solution-processed OLEDs with various electron-transporting host materials. Characteristics of (**A**) capacitance versus voltage and (**B**) transient EL rising of solution-processed phosphorescent orange-red OLEDs. (**C**) Schematic illustration of EOD architecture. (**D**) Electron current density of EODs with various kinds of electron-transporting host materials.

We also fabricated an electron-only device (EOD) [ITO/branched polyethylenimine (PEI) (10 nm)/solution-processed electron-transporting host layer (100 nm)/TPBI (50 nm)/LiF (1 nm)/Al (100 nm)] (Fig. 3C) to investigate the electron-transporting ability of our electron-transporting host materials in the absence of a hole-transporting host (TCTA). A spin-cast thin PEI layer is an effective electron injection layer in OLEDs and an efficient extraction layer in organic photovoltaics (*3*, *48*). Because a thin PEI interfacial layer induces a shift in the vacuum level by surface dipoles, the effective work function of an underlying electrode is reduced, so electrons are easily injected into overlying layers (*3*, *48*). However, we adopted a thin PEI interfacial layer to block the hole injection from the anode into the electron-transporting host layer by reducing the work function of the anode (ITO). Because the deep HOMO energy level (<−6 eV) of electron-transporting hosts and the reduced work function of the ITO anode can effectively inhibit hole injection, we can demonstrate only electron-transporting properties with solution-processed EOD architecture. Results of electron current densities in EODs have identical order with current densities of OLEDs; the OLEDs with 2PTPS exhibited the highest electron current density, and TPBI showed the lowest electron current density (that is, 2PTPS > 3PTPS > 4PTPS > TPBI) (Fig. 3D). The higher electron current density with our host materials means that our host materials have higher electron mobility (μ_e) in the solution-processed film than TPBI. To prove higher electron mobility of our electron-transporting host materials, we additionally performed impedance spectroscopy measurement to determine μ_e of electron-transporting materials (figs. S17 and S18). Calculated μ_e's of TPBI were ~10^{-5} $cm^2/(V{\cdot}s)$, which concurs with those measured by using time of flight in a previous report (fig. S18) (*49*). μ_e of 2PTPS according to electric field range was on the order of ~10^{-4} $cm^2/(V{\cdot}s)$, which is an order higher than that of TPBI. μ_e also increased in the order 2PTPS > 3PTPS > 4PTPS > TPBI (fig. S18); this order is identical with that of current density in solution-processed EODs and OLEDs. The higher μ_e of our electron-transporting host materials increases electron transport in the EML that includes a hole-transporting host (TCTA) [μ_h of TCTA, ~3×10^{-4} $cm^2/(V{\cdot}s)$] (*50*), thereby leveling the charge-carrier balance and broadening the electron-hole recombination zone in the EML. In contrast, the use of a conventional TCTA/TPBI EML provides relatively poor electron-hole balance because TPBI has lower μ_e [~10^{-5} $cm^2/(V{\cdot}s)$] than μ_h of TCTA (*49*).

White OLEDs (WOLEDs) were fabricated using the same methods as those used to fabricate single-color phosphorescent OLEDs except that the EML was composed of two phosphorescent dopants of complementary colors: blue-emitting FIrpic and orange-red–emitting $Bt_2Ir(acac)$ (Fig. 4A). The WOLEDs with 2PTPS and 3PTPS also exhibited superior current density–voltage characteristics (Fig. 4B) and higher CEs and EQEs (device with 2PTPS ~61.5 cd/A, 23.1%; 3PTPS ~74.2 cd/A, 28.5%), than did those with TPBI (~40.5 cd/A, 15.4%) (Fig. 4C, fig. S10, and Table 2); these are the highest recorded device efficiencies among solution-processed WOLEDs without light outcoupling structure reported to date. All WOLEDs fabricated in this work showed good white spectra (Fig. 4D) and Commission Internationale de l'Eclairage chromaticity coordinates of (0.37, 0.46) (color-rendering index, 53) at a normal incidence. Finally, we fabricated highly efficient solution-processed flexible solid-state lighting devices on 5 cm × 5 cm polyethylene terephthalate (PET) substrate (Fig. 4E), which demonstrates a strong potential application of solution-processed OLEDs for solid-state lightings.

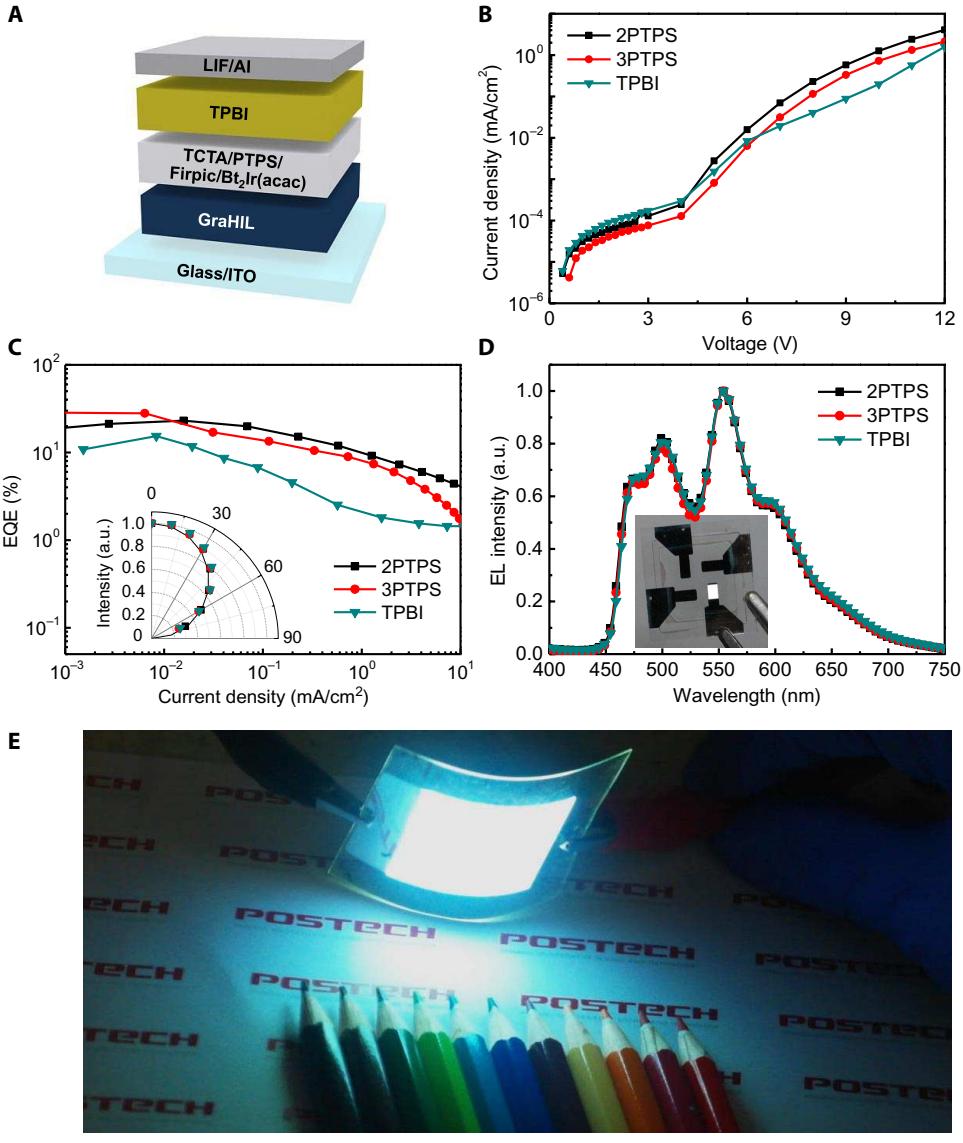

Fig. 4. Electrical and electroluminescent characteristics of solution-processed phosphorescent WOLEDs with various kinds of electron-transporting host materials. (**A**) Schematics of WOLED device architecture. Current density versus voltage (**B**) and EQEs versus current density characteristics (**C**) of phosphorescent WOLEDs (inset: angular EL distributions according to viewing angle). (**D**) EL spectra of phosphorescent WOLEDs (inset: optical image of WOLED with 2PTPS). (**E**) Flexible solution-processed OLED lighting device using 2PTPS on a 5 cm × 5 cm PET substrate.

DISCUSSION

We report efficient simple-structured phosphorescent orange-red, green, blue, and white OLEDs fabricated by a solution process using universal electron-transporting host materials with tetraphenylsilane and pyridine moieties. The wide energy band gaps (4.06 to 4.28 eV) and high E_T's (2.82 to 2.90 eV) of our electron-transporting host materials allow efficient exciton confinement in the EML; the good electron-transporting ability of the materials can provide balanced charge-carrier transport in the mixed-host EML. In *C-V* characterization, the low V_{peak}'s of OLEDs with our materials proved their superior electron-transporting abilities, and faster EL rising in transient EL characterization also demonstrated enhanced electron transport of the mixed-host EML with our host materials compared to that with conventional material (TPBI). Finally, the improved electron current densities of EODs and impedance spectroscopy confirmed that they have higher electron mobilities than TPBI. In addition, the use of the polymeric HIL (GraHIL) that serves gradient and high surface work function reduces the hole injection energy barrier, efficiently blocks exciton quenching at the interface between the HIL and EML, and thereby enables a simple device structure without additional hole-transporting or electron-blocking interlayers. As a result, solution-processed orange-red (~97.5 cd/A, 35.5%), green (~101.5 cd/A, 29.0%), and white OLEDs (~74.2 cd/A, 28.5%) with our electron-transporting hosts exhibited very high electroluminescent efficiencies. We also fabricated a flexible solution-processed solid-state lighting device with our solution-processed phosphorescent WOLEDs. The wide use of our electron-transporting host materials in various-color OLEDs with high device efficiencies demonstrates that our materials and

approaches have potential applications in low-cost, printable OLEDs for solid-state lighting sources and flexible full-color displays.

MATERIALS AND METHODS

Materials

1,3-Dibromobenzene, 2-bromopyridine, tributyltin chloride, 2.5 M *n*-butyllithium, 1.6 M *n*-butyllithium, dichlorodiphenylsilane, 3-pyridineboronic acid, 4-pyridineboronic acid, and tetrakis(triphenylphosphine)palladium were purchased from Aldrich Co. and used as received. The other chemical reagents were common commercial grade and used as received.

Material characterization

Infrared spectra were recorded using a Genesis II FT-IR spectrometer. ^{1}H NMR was recorded using Avance 300-MHz NMR Bruker spectrometers, and chemical shifts were reported in parts per million with tetramethylsilane as internal standard. Thermogravimetric analysis was performed under N_2 on a TA Instrument 2050 thermogravimetric analyzer. The sample was heated at 10°C/min from 50° to 700°C. Differential scanning calorimetry was conducted under N_2 in a TA Instrument 2100 differential scanning calorimeter. The sample was heated at 10°C/min from 30° to 350°C. Mass spectra were measured using a JEOL JMS-700 mass spectrometer. Ultraviolet-visible (UV-vis) absorption spectra were measured using a PerkinElmer LAMBDA-900 UV/VIS/NIR spectrophotometer and an LS-50B luminescence spectrophotometer. The cyclic voltammogram of the material was recorded on an epsilon E3 at room temperature in a 0.1 M solution of tetrabutylammonium perchlorate (Bu_4NClO_4) in acetonitrile under N_2 at a scan rate of 50 mV/s. A Pt wire was used as the counter electrode and an $Ag/AgNO_3$ electrode as the reference electrode.

Device fabrication

Patterned ITO/glass substrates were cleaned by sequential sonication in acetone and isopropanol, each for 30 min. GraHIL (blend of PEDOT/PSS and PFI in a weight ratio of 1:3.6) was coated on the cleaned ITO and baked at 150°C for 30 min. A 40-nm-thick EML was spin-coated from tetrahydrofuran (THF; SAMCHUN chemical Co.) solution in a nitrogen glove box. The EML was composed of a hole-transporting host (TCTA), an electron-transporting host, and phosphorescent dopants. Phosphorescent dopants were Bt2Ir(acac) (orange-red), Ir(ppy)3 (green), and FIrpic (blue). After deposition of EML, a 50-nm-thick TPBI was thermally deposited under high vacuum ($<5 \times 10^{-7}$ torr) as an electron-transporting layer. Finally, LiF (1 nm) and aluminum (100 nm) were sequentially deposited on the TPBI layer. The devices were encapsulated using UV-curable epoxy resin.

Device characterization

The current-voltage-luminance characteristics were measured using a Keithley 236 source measurement unit and a Minolta CS-2000 spectroradiometer. *C-V* characterizations of orange-red phosphorescent OLEDs were conducted using electrochemical impedance spectroscopy (Bio-Logic SP-300). All the devices were biased from 0 to 10 V at a constant frequency of 1000 Hz in the dark. For transient EL characterization of orange-red phosphorescent OLEDs, a constant electrical pulse (200-ms width, 100-Hz frequency) was applied to devices by using a pulse generator (HP 8116A). The emitted light was detected using a photon-counting spectrofluorometer (ISS PC1), and the EL rising output signal was monitored and recorded using an oscilloscope (Agilent Infiniium 54832B DSO).

SUPPLEMENTARY MATERIALS

Supplementary material for this article is available at http://advances.sciencemag.org/cgi/content/full/2/10/e1601428/DC1

Supplementary Materials and Methods

table S1. Physical properties of 2PTPS, 3PTPS, and 4PTPS.

table S2. Work functions with a function of PFI concentration in GraHIL compositions measured by UV photoelectron spectroscopy in air (AC2, Riken Keiki Co. Ltd.).

table S3. Calculated HOMO, LUMO, E_T, and dipole moment.

fig. S1. CV spectra of 2PTPS, 3PTPS, and 4PTPS.

fig. S2. UV-vis absorption and photoluminescence of 2PTPS.

fig. S3. UV-vis absorption and photoluminescence of 3PTPS.

fig. S4. UV-vis absorption and photoluminescence of 4PTPS.

fig. S5. Phosphorescence spectra of 2PTPS, 3PTPS, and 4PTPS at 77 K.

fig. S6. Chemical structure of PFI.

fig. S7. X-ray photoelectron spectroscopy molecular depth profiles of the GraHIL.

fig. S8. Angular EL distributions according to viewing angles of solution-processed OLEDs.

fig. S9. Normalized EL spectra according to viewing angles of solution-processed OLEDs.

fig. S10. CEs of solution-processed OLEDs.

fig. S11. Photoluminescence of mixed-host EMLs and UV-vis absorption of phosphorescent dopants.

fig. S12. Photoluminescence of mixed-host EMLs according to concentration of phosphorescent dopant.

fig. S13. Capacitance versus voltage characteristics of mixed-host EMLs.

fig. S14. Current density versus voltage of OLEDs using TCTA/2PTPS EML according to phosphorescent dopants.

fig. S15. Schematic illustrations of device structure for solution-processed single-carrier devices.

fig. S16. Current density versus voltage of single-carrier devices according to phosphorescent dopants.

fig. S17. Negative differential susceptance versus frequency of EODs.

fig. S18. Calculated electron mobilities of 2PTPS, 3PTPS, 4PTPS, and TPBI.

fig. S19. Density functional theory calculations of 2PTPS, 3PTPS, and 4PTPS.

REFERENCES AND NOTES

1. J. Kido, M. Kimura, K. Nagai, Multilayer white light-emitting organic electroluminescent device. *Science* **267**, 1332–1334 (1995).
2. S. Reineke, F. Lindner, G. Schwartz, N. Seidler, K. Walzer, B. Lüssem, K. Leo, White organic light-emitting diodes with fluorescent tube efficiency. *Nature* **459**, 234–238 (2009).
3. Y. Zhou, C. Fuentes-Hernandez, J. Shim, J. Meyer, A. J. Giordano, H. Li, P. Winget, T. Papadopoulos, H. Cheun, J. Kim, M. Fenoll, A. Dindar, W. Haske, E. Najafabadi, T. M. Khan, H. Sojoudi, S. Barlow, S. Graham, J.-L. Brédas, S. R. Marder, A. Khan, B. Kippelen, A universal method to produce low–work function electrodes for organic electronics. *Science* **336**, 327–332 (2012).
4. T.-H. Han, Y. Lee, M.-R. Choi, S.-H. Woo, S.-H. Bae, B. H. Hong, J.-H. Ahn, T.-W. Lee, Extremely efficient flexible organic light-emitting diodes with modified graphene anode. *Nat. Photonics* **6**, 105–110 (2012).
5. M. G. Helander, Z. B. Wang, J. Qiu, M. T. Greiner, D. P. Puzzo, Z. W. Liu, Z. H. Lu, Chlorinated indium tin oxide electrodes with high work function for organic device compatibility. *Science* **332**, 944–947 (2011).
6. M. C. Gather, A. Köhnen, K. Meerholz, White organic light-emitting diodes. *Adv. Mater.* **23**, 233–248 (2011).
7. DuPont's OLED material hits million-hour lifetime. *Nat. Photonics* **3**, 441 (2009).
8. L. Duan, L. Hou, T.-W. Lee, J. Qiao, D. Zhang, G. Dong, L. Wang, Y. Qiu, Solution processable small molecules for organic light-emitting diodes. *J. Mater. Chem.* **20**, 6392–6407 (2010).
9. T.-W. Lee, T. Noh, H.-W. Shin, O. Kwon, J.-J. Park, B.-K. Choi, M.-S. Kim, D. W. Shin, Y.-R. Kim, Characteristics of solution-processed small-molecule organic films and light-emitting diodes compared with their vacuum-deposited counterparts. *Adv. Funct. Mater.* **19**, 1625–1630 (2010).
10. M. Singh, H. M. Haverinen, P. Dhagat, G. E. Jabbour, Inkjet printing—Process and its applications. *Adv. Mater.* **22**, 673–685 (2010).
11. F.So, B. Krummacher, M. K. Mathai, D. Poplavskyy, S. A. Choulis, V.-E. Choong, Recent progress in solution processable organic light emitting devices. *J. Appl. Phys.* **102**, 091101 (2007).
12. R. H. Friend, R. W. Gymer, A. B. Holmes, J. H. Burroughes, R. N. Marks, C. Taliani, D. D. C. Bradley, D. A. Dos Santos, J. L. Brédas, M. Lögdlund, W. R. Salaneck, Electroluminescence in conjugated polymers. *Nature* **397**, 121–128 (1999).
13. M. C. Gather, A. Köhnen, A. Falcou, H. Becker, K. Meerholz, Solution-processed full-color polymer organic light-emitting diode displays fabricated by direct photolithography. *Adv. Funct. Mater.* **17**, 191–200 (2007).

14. B. R. Lee, J.-w. Kim, D. Kang, D. W. Lee, S.-J. Ko, H. J. Lee, C.-L. Lee, J. Y. Kim, H. S. Shin, M. H. Song, Highly efficient polymer light-emitting diodes using graphene oxide as a hole transport layer. *ACS Nano* **6**, 2984–2991 (2012).
15. C.-G. Zhen, Z.-K. Chen, Q.-D. Liu, Y.-F. Dai, R. Y. C. Shin, S.-Y. Chang, J. Kieffer, Fluorene-based oligomers for highly efficient and stable organic blue-light-emitting diodes. *Adv. Mater.* **21**, 2425–2429 (2009).
16. N. Rehmann, D. Hertel, K. Meerholz, H. Becker, S. Heun, Highly efficient solution-processed phosphorescent multilayer organic light-emitting diodes based on small-molecule hosts. *Appl. Phys. Lett.* **91**, 103507 (2007).
17. S. Gong, Q. Fu, Q. Wang, C. Yang, C. Zhong, J. Qin, D. Ma, Highly efficient deep-blue electrophosphorescence enabled by solution-processed bipolar tetraarylsilane host with both a high triplet energy and a high-lying HOMO Level. *Adv. Mater.* **23**, 4956–4959 (2011).
18. S. Ye, Y. Liu, J. Chen, K. Lu, W. Wu, C. Du, Y. Liu, T. Wu, Z. Shuai, G. Yu, Solution-processed solid solution of a novel carbazole derivative for high-performance blue phosphorescent organic light-emitting diodes. *Adv. Mater.* **22**, 4167–4171 (2010).
19. E. Ahmed, T. Earmme, S. A. Jenekhe, New solution-processable electron transport materials for highly efficient blue phosphorescent OLEDs. *Adv. Funct. Mater.* **21**, 3889–3899 (2011).
20. T. Earmme, E. Ahmed, S. A. Jenekhe, Solution-processed highly efficient blue phosphorescent polymer light-emitting diodes enabled by a new electron transport material. *Adv. Mater.* **22**, 4744–4748 (2010).
21. M. Cai, T. Xiao, E. Hellerich, Y. Chen, R. Shinar, J. Shinar, High-efficiency solution-processed small molecule electrophosphorescent organic light-emitting diodes. *Adv. Mater.* **23**, 3590–3596 (2011).
22. J.-H. Jou, M.-F. Hsu, W.-B. Wang, C.-L. Chin, Y.-C. Chung, C.-T. Chen, J.-J. Shyue, S.-M. Shen, M.-H. Wu, W.-C. Chang, C.-P. Liu, S.-Z. Chen, H.-Y. Chen, Solution-processable, high-molecule-based trifluoromethyl-iridium complex for extraordinarily high efficiency blue-green organic light-emitting diode. *Chem. Mater.* **21**, 2565–2567 (2009).
23. N. Aizawa, Y.-J. Pu, H. Sasabe, J. Kido, Solution-processable carbazole-based host materials for phosphorescent organic light-emitting diodes. *Org. Electron.* **13**, 2235–2242 (2012).
24. B. Zhang, G. Tan, C.-S. Lam, B. Yao, C.-L. Ho, L. Liu, Z. Xie, W.-Y. Wong, J. Ding, L. Wang, High-efficiency single emissive layer white organic light-emitting diodes based on solution-processed dendritic host and new orange-emitting iridium complex. *Adv. Mater.* **24**, 1873–1877 (2012).
25. G. Liaptsis, D. Hertel, K. Meerholz, Solution processed organic double light-emitting layer diode based on cross-linkable small molecular systems. *Angew. Chem. Int. Ed. Engl.* **52**, 9563–9567 (2013).
26. K. S. Yook, J. Y. Lee, Small molecule host materials for solution processed phosphorescent organic light-emitting diodes. *Adv. Mater.* **26**, 4218–4233 (2014).
27. S. O. Jung, J.-W. Park, D. M. Kang, J.-S. Kim, S.-J. Park, P. Kang, H.-Y. Oh, J.-H. Yang, Y.-H. Kim, S.-K. Kwon, New amorphous hole blocking materials for high efficiency OLEDs. *J. Nanosci. Nanotechnol.* **8**, 4838–4841 (2008).
28. L. Xiao, S.-J. Su, Y. Agata, H. Lan, J. Kido, Nearly 100% internal quantum efficiency in an organic blue-light electrophosphorescent device using a weak electron transporting material with a wide energy cap. *Adv. Mater.* **21**, 1271–1274 (2009).
29. S. Tokito, T. Iijima, Y. Suzuri, H. Kita, T. Tsuzuki, F. Sato, Confinement of triplet energy on phosphorescent molecules for highly-efficient organic blue-light-emitting devices. *Appl. Phys. Lett.* **83**, 569–571 (2003).
30. T.-H. Han, M.-R. Choi, S.-H. Woo, S.-Y. Min, C.-L. Lee, T.-W. Lee, Molecularly controlled interfacial layer strategy toward highly efficient simple-structured organic light-emitting diodes. *Adv. Mater.* **24**, 1487–1493 (2012).
31. T.-W. Lee, Y. Chung, O. Kwon, J.-J. Park, Self-organized gradient hole injection to improve the performance of polymer electroluminescent devices. *Adv. Funct. Mater.* **17**, 390–396 (2007).
32. M. E. Kondakova, T. D. Pawlik, R. H. Young, D. J. Giesen, D. Y. Kondakov, C. T. Brown, J. C. Deaton, J. R. Lenhard, K. P. Klubek, High-efficiency, low-voltage phosphorescent organic light-emitting diode devices with mixed host. *J. Appl. Phys.* **104**, 094501 (2008).
33. Q. Fu, J. Chen, C. Shi, D. Ma, Solution-processed small molecules as mixed host for highly efficient blue and white phosphorescent organic light-emitting diodes. *ACS Appl. Mater. Interfaces* **4**, 6579–6586 (2012).
34. A. Graf, P. Liehm, C. Murawski, S. Hofmann, K. Leo, M. C. Gather, Correlating the transition dipole moment orientation of phosphorescent emitter molecules in OLEDs with basic material properties. *J. Mater. Chem. C* **2**, 10298–10304 (2014).
35. K.-H. Kim, C.-K. Moon, J.-H. Lee, S.-Y. Kim, J.-J. Kim, Highly efficient organic light-emitting diodes with phosphorescent emitters having high quantum yield and horizontal orientation of transition dipole moments. *Adv. Mater.* **26**, 3844–3847 (2014).
36. S.-Y. Kim, W.-I. Jeong, C. Mayr, Y.-S. Park, K.-H. Kim, J.-H. Lee, C.-K. Moon, W. Brütting, J.-J. Kim, Organic light-emitting diodes with 30% external quantum efficiency based on a horizontally oriented emitter. *Adv. Funct. Mater.* **23**, 3896–3900 (2013).
37. Y.-H. Huang, W.-L. Tsai, W.-K. Lee, M. Jiao, C.-Y. Lu, C.-Y. Lin, C.-Y. Chen, C.-C. Wu, Unlocking the full potential of conducting polymers for high-efficiency organic light-emitting devices. *Adv. Mater.* **27**, 929–934 (2015).
38. Y.-S. Park, S. Lee, K.-H. Kim, S.-Y. Kim, J.-H. Lee, J.-J. Kim, Exciplex-forming co-host for organic light-emitting diodes with ultimate efficiency. *Adv. Funct. Mater.* **23**, 4914–4920 (2013).
39. J.-H. Lee, S. Lee, S.-J. Yoo, K.-H. Kim, J.-J. Kim, Langevin and trap-assisted recombination in phosphorescent organic light emitting diodes. *Adv. Funct. Mater.* **24**, 4681–4688 (2014).
40. W. Song, J. Y. Lee, Light emission mechanism of mixed host organic light-emitting diodes. *Appl. Phys. Lett.* **106**, 123306 (2015).
41. A. J. Mäkinen, I. G. Hill, Z. H. Kafafi, Vacuum level alignment in organic guest-host systems. *J. Appl. Phys.* **92**, 1598 (2002).
42. X. Gong, J. C. Ostrowski, D. Moses, G. C. Bazan, A. J. Heeger, Electrophosphorescence from a polymer guest–host system with an Iridium complex as guest: Förster energy transfer and charge trapping. *Adv. Funct. Mater.* **13**, 439–444 (2003).
43. J. Lee, J.-I. Lee, J. Y. Lee, H. Y. Chu, Enhanced efficiency and reduced roll-off in blue and white phosphorescent organic light-emitting diodes with a mixed host structure. *Appl. Phys. Lett.* **94**, 193305 (2009).
44. M. Mesta, M. Carvelli, R. J. de Vries, H. van Eersel, J. J. M. van der Holst, M. Schober, M. Furno, B. Lüssem, K. Leo, P. Loebl, R. Coehoorn, P. A. Bobbert, Molecular-scale simulation of electroluminescence in a multilayer white organic light-emitting diode. *Nat. Mater.* **12**, 652–658 (2013).
45. P.-I. Shih, C.-H. Chien, C.-Y. Chuang, C.-F. Shu, C.-H. Yang, J.-H. Chen, Y. Chi, Novel host material for highly efficient blue phosphorescent OLEDs. *J. Mater. Chem.* **17**, 1692–1698 (2007).
46. V. Shrotriya, Y. Yang, Capacitance-voltage characterization of polymer light-emitting diodes. *J. Appl. Phys.* **97**, 054504 (2005).
47. T.-H. Han, W. Song, T.-W. Lee, Elucidating the crucial role of hole injection layer in degradation of organic light-emitting diodes. *ACS Appl. Mater. Interfaces* **7**, 3117–3125 (2015).
48. Y.-H. Kim, T.-H. Han, H. Cho, S.-Y. Min, C.-L. Lee, T.-W. Lee, Polyethylene imine as an ideal interlayer for highly efficient inverted polymer light-emitting diodes. *Adv. Funct. Mater.* **24**, 3808–3814 (2014).
49. W.-Y. Hung, T.-H. Ke, Y.-T. Lin, C.-C. Wu, T.-H. Hung, T.-C. Chao, K.-T. Wong, C.-I. Wu, Employing ambipolar oligofluorene as the charge-generation layer in time-of-flight mobility measurements of organic thin films. *Appl. Phys. Lett.* **88**, 064102 (2006).
50. J.-W. Kang, S.-H. Lee, H.-D. Park, W.-I. Jeong, K.-M. Yoo, Y.-S. Park, J.-J. Kim, Low roll-off of efficiency at high current density in phosphorescent organic light emitting diodes. *Appl. Phys. Lett.* **90**, 223508 (2007).

Acknowledgments

Funding: This work was supported by the National Research Foundation of Korea grant funded by the Korean government (Ministry of Science, ICT and Future Planning) (NRF-2016R1A3B1908431 and NRF-2015R1A2A1A10055620). **Author contributions:** T.-H.H. designed and conducted most of the experiments, analyzed all the data, and prepared the manuscript. M.-R.C. assisted in experiments and preparation of the manuscript. C-.W.J. synthesized materials. Y.-H.K. and S.-K.K. designed synthesis and analysis of materials and assisted in the preparation of the manuscript. T.-W.L. initiated the study, designed all the experiments, analyzed all the data, and assisted in preparing the manuscript. All authors discussed the results and contributed to the paper. **Competing interests:** The authors declare that they have no competing interests. **Data and materials availability:** All data needed to evaluate the conclusions in the paper are present in the paper and/or the Supplementary Materials. Additional data related to this paper may be requested from the authors.

Submitted 23 June 2016
Accepted 27 September 2016
Published 28 October 2016
10.1126/sciadv.1601428

Citation: T.-H. Han, M.-R. Choi, C.-W. Jeon, Y.-H. Kim, S.-K. Kwon, T.-W. Lee, Ultrahigh-efficiency solution-processed simplified small-molecule organic light-emitting diodes using universal host materials. *Sci. Adv.* **2**, e1601428 (2016).

Science Advances

Ultrahigh-efficiency solution-processed simplified small-molecule organic light-emitting diodes using universal host materials

Tae-Hee Han, Mi-Ri Choi, Chan-Woo Jeon, Yun-Hi Kim, Soon-Ki Kwon and Tae-Woo Lee

Sci Adv **2** (10), e1601428.
DOI: 10.1126/sciadv.1601428

Science Advances (ISSN 2375-2548) is published by the American Association for the Advancement of Science, 1200 New York Avenue NW, Washington, DC 20005. The title *Science Advances* is a registered trademark of AAAS.